Optical and Quantum Electronics (2024) 56:1730
https://doi.org/10.1007/s11082-024-07614-x

Numerical modeling of SNSPD absorption utilizing optical conductivity with quantum corrections

Martin Baránek[1] · Pavol Neilinger[1,2] · Samuel Kern[1] · Miroslav Grajcar[1,2]

Received: 9 August 2024 / Accepted: 25 September 2024 / Published online: 9 October 2024

Abstract
Superconducting nanowire single-photon detectors are widely used in various fields of physics and technology, due to their high efficiency and timing precision. Although, in principle, their detection mechanism offers broadband operation, their wavelength range has to be optimized by the optical cavity parameters for a specific task. We present a study of the optical absorption of a superconducting nanowire single photon detector with an optical cavity. The optical properties of the niobium nitride films, measured by spectroscopic ellipsometry, were modeled using the Drude–Lorentz model with quantum corrections. The numerical simulations of the optical response of the detectors show that the wavelength range of the detector is not solely determined by its geometry, but the optical conductivity of the disordered thin metallic films contributes considerably. This contribution can be conveniently expressed by the ratio of imaginary and real parts of the optical conductivity. This knowledge can be utilized in detector design.

Keywords SNSPD · Optical properties · Optical absorption · Thin film · Optical cavity

Pavol Neilinger, Samuel Kern and Miroslav Grajcar have contributed equally to this work.

✉ Martin Baránek
martin.baranek@fmph.uniba.sk

Pavol Neilinger
pavol.neilinger@fmph.uniba.sk

Samuel Kern
samuel.kern@fmph.uniba.sk

Miroslav Grajcar
grajcar@fmph.uniba.sk

[1] Department of Experimental Physics, Comenius University, Mlynská Dolina F1, 84248 Bratislava, Slovakia

[2] Institute of Physics, Slovak Academy of Sciences, Dúbravská cesta 9, 84511 Bratislava, Slovakia

1 Introduction

Strengthening the security of digital communication channels by building Quantum Key Distribution (QKD) infrastructure is an ongoing effort worldwide (Chen et al. 2021; Ribezzo et al. 2023). Most QKD systems are based on entangled photon pairs as quantum bits and utilize the existing, low-loss fiber optical infrastructure (Aktas et al. 2016). To implement an efficient algorithm, a single-photon detector with a high overall detection efficiency, low dark counts, and high speed is required (Shibata et al. 2014). The State-of-the-art detectors that fulfill these requirements are the superconducting nanowire single-photon detectors (SNSPD) (Goĺtsman et al. 2001). They are superior in terms of detection efficiency and dark count rates to other types (Esmaeil Zadeh, Iman et al. 2021), such as the Avalanche Photodiodes (APD) (Renker 2006), and do not require sub-kelvin temperatures, as the Transition Edge Sensors (TES) (Cabrera et al. 1998) do. Moreover, their superior properties make them beneficial in a broad range of applications in different areas of physics, for example, physical chemistry and spectroscopy (Lau et al. 2023), fluorescent luminescence (Wang et al. 2019), or fast space-to-ground communication (Hao et al. 2024) often requiring a lower wavelength range. The detector's wavelength can be optimized by its design depending on the required spectral range. This is also important in the implementation of modern quantum networks (Aktas et al. 2016; Lim et al. 2010) as not just the detection efficiency of the detector, but its bandwidth is a relevant parameter.

The working principle of SNSPD is straightforward: a nanowire in the superconducting state is current-biased close to the edge of the normal metal transition. The absorption of a single photon results in the destruction of superconductivity at some place along the nanowire. Due to the current bias, the normal state region expands, which results in a voltage pulse across the nanowire. These nanowires are fabricated on 6–15 nm thick, highly disordered superconductors, such as Niobium Nitride (Zhang et al. 2017), Titanium Niobium Nitride (Chang et al. 2021), Tungsten Silicide (Marsili et al. 2013) and their width is in the range of 30–200 nm.

The overall system detection efficiency (SDE) of detectors is determined by the efficiency of the photon coupling to the active area of the detector η_{coupling}, the photon absorption efficiency of the superconductor η_{abs}, and by the above-described efficiency of transformation of the absorbed photon to electric signal $\eta_{\text{intrinsic}}$ and is given as You (2020):

$$\text{SDE} = \eta_{\text{coupling}} \cdot \eta_{\text{abs}} \cdot \eta_{\text{intrinsic}}, \tag{1}$$

The absorption of a nanowire (thin film) η_{abs} on bare substrate is insufficient (below 30%, Fig. 2). To increase the absorption at the desired wavelength ($\lambda = 1550$ nm) the nanowires are commonly fabricated in an optical resonator, at the cost of limiting its bandwidth. A common choice is a $\lambda/4$ resonant cavity (Redaelli et al. 2016).

This resonator consists of a thin dielectric layer with thickness d_1, matching its optical length Λ with $\lambda/4$ of the desired light's wavelength. The nanowire is fabricated on one side of the dielectric and the other side is covered with a low-loss mirror metallic layer (as shown in Fig. 1). The resonator enhances the absorption of the photons in the nanowire close to 100% (Fig. 2) by creating an antinode of the electric field of TE mode in the superconductor. The detectable light is guided by an optical fiber to this structure.

To properly model the optical properties of this structure, and thus to maximize the absorption η_{abs} in the nanowire, not only has the dielectric thickness d_1 to be optimized, but the precise optical properties of the disordered metal have to be considered. However, their optical properties in the metallic state are not trivial due to the presence of quantum corrections,

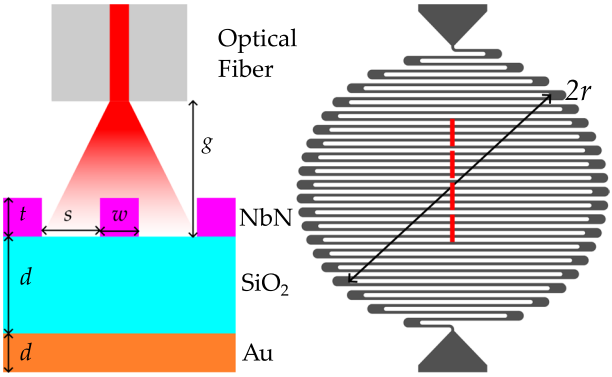

Fig. 1 Scheme of the SNSPD with coupled optical fiber. Nanowire has thickness t, width w, and spacing s. Optical $\lambda/4$ resonator consists of a dielectric spacer with thickness d_1 and a gold reflector with d_2. The gap between optical fiber and nanowire is g. Right: Top-down view of the nanowire of diameter $2r$, with red line showing the position of the cross-sectional view

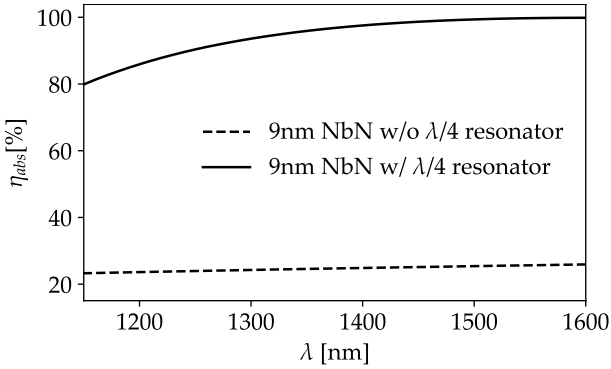

Fig. 2 Nanowire optical absorption η_{abs} on bare sapphire substrate and on $\lambda/4$ resonator

which the standard Drude model fails to describe (Neilinger et al. 2019). This means that, to model their optical absorption, the optical properties of the specific thin film have to be either measured in the infrared spectra, or the right optical model - or an extrapolation method - has to be chosen, if measurements in the required range are not accessible.

In this paper, we investigate the dependence of the optical absorption of NbN nanowires in $\lambda/4$ resonant cavity on film thickness and nanowire design. The optical conductivity of a set of NbN films was determined from spectroscopic ellipsometry in the visible range, and they were fitted by the modified Drude–Lorentz model, which takes the quantum corrections into account, which is presented in preprint by Kern et al. (2024), and provides an excellent fit of these conductivities. The presence of quantum corrections in the IR range results in a strong wavelength and thickness dependence of the optical properties of NbN films. The obtained optical fits and thickness dependencies of its parameters are used to model the absorption spectra of nanowires. The presented approach can be applied to other disordered films, such as MoC and NbTiN. The optical properties of the latter (Banerjee et al. 2018) are almost identical to the properties of NbN.

2 Optical properties of NbN films

Niobium nitride samples were deposited by means of Pulsed Laser Deposition (Volkov et al. 2019) from a 99% pure niobium target on top of single-side polished sapphire substrate in a nitrogen atmosphere with 1% of hydrogen. The film thickness varied from 8 up to 22 nm. The optical conductivities of our films were determined from spectroscopic ellipsometry measured in wavelength range from 400 to 1000 nm at room temperature.

In Kern et al. (2024), the quantum corrections to the optical conductivity of these NbN films were thoroughly studied. These corrections are arising from localization and interaction effects both having a square root energy dependence (Efros and Pollak 2012). The optical conductivity $\tilde{\sigma} = \sigma_1 + i\sigma_2$ is described by the modified Drude–Lorentz model in the form:

$$\sigma_1(\omega) = \frac{\sigma_D}{1 + \left(\frac{\Omega}{\Gamma}\right)^2}\left(1 - \mathcal{Q}^2\left(1 - \sqrt{\frac{\Omega}{\Gamma}}\right)e^{-\frac{1}{2}\left(\frac{\Omega}{\Gamma}\right)^2}\right) + \frac{\sigma_L}{1 + \left(\frac{\Omega_L^2 - \Omega^2}{\Omega\Gamma_L}\right)^2}, \tag{2}$$

$$\sigma_2(\omega) = \mathcal{H}[\sigma_1(\omega)] - (\varepsilon_\infty - 1)\varepsilon_0\omega \tag{3}$$

respectively.

Here, σ_D is the Drude conductivity, Γ is the electron relaxation rate and $\mathcal{Q}$ is the strength of the quantum corrections, also referred to as quantumness. The generalized frequency entering the square root correction is defined as: $\Omega = \sqrt{\omega^2 + (k_B T/\hbar)^2}$, which includes the temperature smearing at low frequencies. $\mathcal{H}[\sigma_1(\omega)]$ denotes the Hilbert transform of Eq. 2, i.e. its Kramers–Kronig image (a closed formula can be found in Kern et al. (2024)).

The second term in the RHS of the Eq. 2 describes the interband transition at Ω_L, with strength σ_L, and width Γ_L. This formula, especially its first term, describes the anomalous conductivity suppression in the IR range and below, which is characteristic of these films. The optical conductivity for films with different thicknesses is shown in Fig. 3 The same result can be represented by σ_1 vs. σ_2 plots in Fig. 4, where the wavelength dependence is color-coded. The solid spirals are the fits with Eqs. 2, 3. The fitted parameters are listed in Table 1.

As can be seen in Fig. 3, the Drude conductivity σ_D varies weakly with thickness, even though the DC conductivity $\sigma_1(\omega = 0)$ decreases for thinner films. This is caused by the suppression of the conductivity by quantum corrections, which can be expressed according Eq. 2 as $\sigma_1(\omega = 0) \approx (1 - \mathcal{Q}^2)\sigma_D$. The extrapolated DC conductivity $\sigma_1(\omega = 0)$ fits well to the values determined by sheet resistance measurement (see circles in Fig. 3). The quantumness $\mathcal{Q}$ is strongly thickness dependent. This reflects the commonly observed suppression of DC conductivity and, most importantly, the significant changes in the optical properties of films, especially in the IR range. By lowering the thickness, the real part of the IR range conductivity is suppressed and the imaginary part changes its sign. The dielectric function

$$\varepsilon_r(\omega) = \varepsilon_1 + i\varepsilon_2 = 1 + i\tilde{\sigma}(\omega)/(\epsilon_0\omega) \tag{4}$$

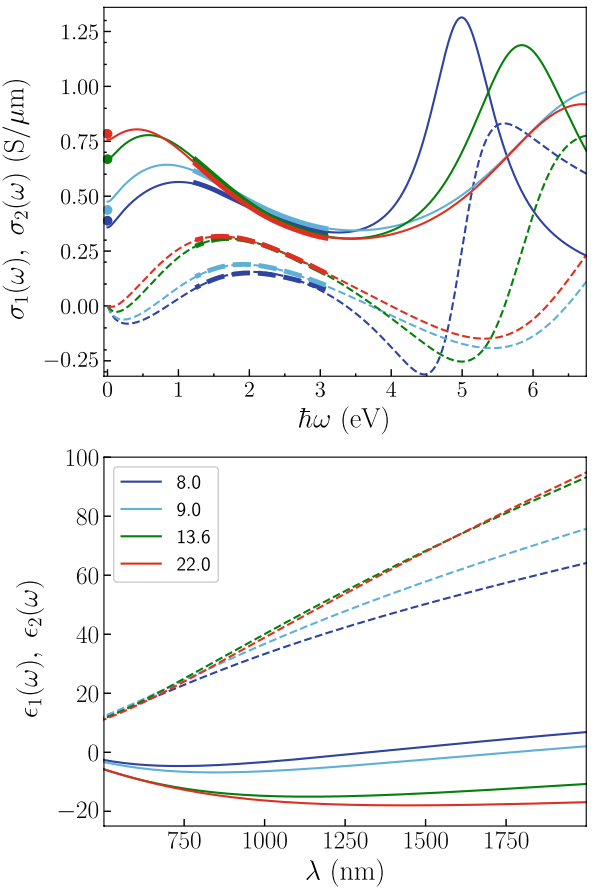

Fig. 3 Specific conductivity (top) and permittivity (bottom) of thin NbN films, consisting of real (solid line) and imaginary (dashed line) parts. Thick lines are the result of spectroscopic ellipsometry measurement, and thin lines result from the model described above. Dots at zero frequency are the room temperature DC conductivities

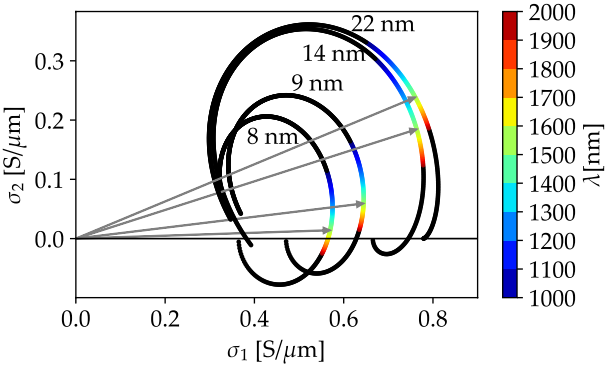

Fig. 4 Wavelength-dependent real and imaginary part of conductivity for films with various thicknesses. The arrows show the mismatch in the simple rescaling of the conductivities, easily visible by the change in the angle θ_0 of arrows, which point at the conductivity at 1550 nm

for various film thicknesses is plotted in Fig. 3. The known thickness dependence of these parameters allows us to conveniently model the optical properties of SNSPDs. The complex refraction index can be expressed in terms of permittivity, as:

Table 1 Parameters of optical model Eq. (2) obtained from the ellipsometric data fit

d[nm]	σ_D (MS/m)	$\hbar\Gamma$ (eV)	$\mathcal{Q}$	σ_L (MS/m)	$\hbar\Gamma_L$ (eV)	$\hbar\Omega_L$ (eV)
8	0.77	2.1	0.7	0.9	1.0	6.13
9	0.84	2.0	0.6	0.95	1.1	6.14
14	1.00	1.76	0.66	1.12	0.56	5.19
22	0.94	1.77	0.50	1.07	0.68	5.54

$$\tilde{n} = \sqrt{\varepsilon_r(\omega)}, \tag{5}$$

It is important to note, that not just the magnitude of the conductivity changes with the thickness, but the ratio of real to imaginary parts changes as well. This is easily visible by the change of the angle of the arrow pointing to the conductivity at $\lambda_0 = 1550$ nm in Fig. 4. This angle is defined by the tangent of real and imaginary parts of the optical conductivity as $\tan\theta_0 = \sigma_2(\lambda_0)/\sigma_1(\lambda_0)$ and is a characteristic of the films for a given thickness - it does not depend on the fill factor of the nanowire, since scaling the conductivity scales both real and imaginary part.

3 Optical absorption simulations

We studied the effect of the film's conductivity on the absorption spectra of SNSPD with a similar detector design to Ref. Chang et al. (2021). The numerical simulations were carried out in a commercial frequency-domain EM solver (COMSOL 2023). The air gap between the fiber and the surface of the detector leads to additional Fabry–Peròt resonances superposing the absorption spectra of the $\lambda/4$ resonator. This could be expressed in the wavelength dependence of the coupling parameter $\eta_{\text{coupling}}(\lambda)$. In our 2D simulations, the optical fiber output is modeled as a plane wave coupled to air and we assume infinite size of the detector in the plane perpendicular to the light propagation, which corresponds to the ideal coupling $\eta_{\text{coupling}} = 1$ and allows us to focus on the absorption in the nanowire η_{abs}.

The optical absorption of the SNSPD can be described by the effective impedance model (Driessen, E. F. C. et al. 2009), which approximates the thin superconducting meander as a lumped element effective homogeneous medium, with effective sheet conductance $\tilde{G} = G_1 + iG_2$:

$$\tilde{G} = \tilde{\sigma}\frac{w}{w+s}t\ [\text{S}/\square], \tag{6}$$

where $\tilde{\sigma}(t)$ is the optical conductivity (in units of S/m) of the NbN film with thickness t, and the ratio $f = w/(w+s)$ is the fill factor. This approximation is valid for the width and the thickness of the nanowires $w, t \ll \lambda$. As these parameters are usually $w \sim 30$–200 nm, $t \sim 5$–22 nm, and $s \sim 50$–300 nm, this approximation holds well for $\lambda > 1$ µm. The validity of this approximation is demonstrated by numerical modeling of the absorption spectra of a detector with different nanowire widths and constant fill factor $f = 0.5$, shown in Fig. 5. The absorption spectra are almost identical for $w \lesssim 400$nm. The negligible differences in the absorption maximum ($< 0.5\%$) and its wavelength (< 50 nm) may originate in simulation mesh discretization. The $\approx 1\%$ losses originate in the Au layer with $d_2 = 100$ nm.

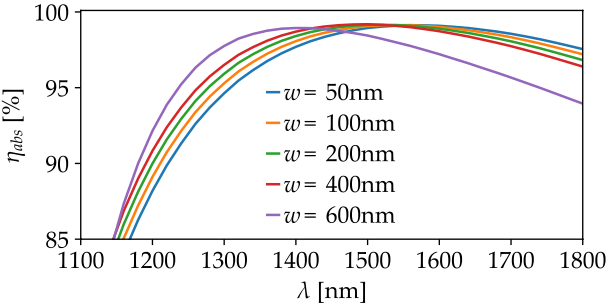

Fig. 5 Simulated absorption spectra of the detector for different nanowire widths and constant fill factor $f = 0.5$

In Fig. 6, we present the absorption spectra of a detector with 100 nm width NbN nanowire of different thicknesses $t = 8-22$ nm on SiO_2 layer with thickness d_1= 250 nm. The absorption maximum corresponding to the optical length of an ideal $\lambda/4$ resonator is $4\Lambda = 4nd_1 \approx 1600$ nm. For each thickness, the fill factor f was tuned to maximize the absorption at $\lambda_0 = 1550$ nm. The maximal absorptions at λ_0, and the wavelength of the absolute maximal absorption λ are listed in Table 2. Note, that for this analysis, the optical properties of NbN films were extracted from ellipsometric measurements on films deposited on c-cut sapphire substrate. The optical properties of films deposited on different substrates, for example, SiO_2 or Si_3N_4, can differ. However, the presented wavelength shift is a general phenomenon and can be estimated for any combination of film and dielectric material, as we will show below.

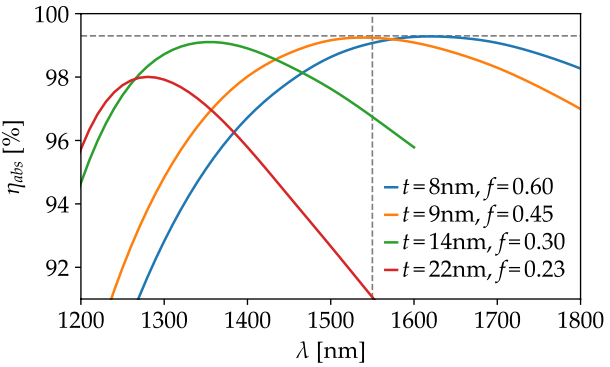

Fig. 6 Simulated absorption spectra of nanowires with different thicknesses for fill factor maximizing absorption at 1550 nm

Table 2 Simulated maximum absorption at 1550 nm and the optimized fill factor for 1550 nm, wavelength of maximum absorption, and maximum absorption value for different thicknesses

250 nm SiO_2, $4\Lambda = 1600$ nm					
d[nm]	σ_2/σ_1 @1550 nm	max(η_{abs}) @1550 nm (%)	Fill factor	λ_{max} (nm)	max (η_{abs}) (%)
8	0.025	99.1	0.6	1650	99.3
9	0.092	99.2	0.45	1550	99.2
14	0.242	96.8	0.3	1350	99.1
22	0.314	91.5	0.225	1250	97.9

The absorption spectra for $t = 8$, 9, 14, 22 nm are shown in Fig. 6. As it is visible, due to the thickness dependence of the optical conductivity (refraction index), the thickness of the film significantly shifts the position of the absorption maxima and changes the shape of the absorption spectra. The maximum of the absorption value $\max(\eta_{abs})$, at its peak wavelength λ_{max}, is also lowered for thicker films due to the increased reflection, but it is negligible compared to the drop of absorption at the desired wavelength $\lambda_0 = 1550$ nm. To study how G_1 and G_2 separately affect the absorption spectra, we simulated the absorption of the nanowire with $w = 100$ nm, $s = 100$ nm ($f = 0.5$), $t = 10$ nm on $d_1 = 250$ nm SiO_2 dielectric and $d_2 = 100$ nm Au reflector.

The absorption spectra for varying G_1 and constant $G_2 = 0$ reveal that the real part of the effective sheet conductance G_1 (σ_1, respectively) mainly affects the value of the absorption maxima, but not their position λ_{max}, shown in Fig. 7a. On the other hand, variation of $G_2(\sigma_2$, respectively) for constant G_1 results in the shift of absorption peak λ_{max}, shown in Fig. 7b. The simulated range of $\tan\theta$ is approx. 0–0.4, which is comparable to the values of our films (0–0.32). Thus, the resonant absorption peak of the detector is shifted by the imaginary part of the conductance towards lower values and thus, its wavelength λ_{max} is not solely determined by the thickness of the dielectric layer, as one could simply assume. This effect, governed by $\tan\theta$, is universal and should be present in any thin film with similar values of $\tan\theta$.

The dependence of $1/\lambda_{max}$ on the conductivity of the NbN films represented by $\tan\theta$ is linear for a broad range of $\tan\theta$ as is visible in Fig. 8, and can be approximated as:

$$\frac{1}{\lambda_{\max}(\sigma_2)} = \frac{1}{\lambda_{\max}(\sigma_2 = 0)} + \frac{1}{\lambda_c}\tan\theta, \tag{7}$$

where λ_c is a fitting parameter. The value λ_c is governed by the optical properties of the dielectric layer and its thickness. For the studied geometry of the detector on SiO_2, $\lambda_c \sim 4.2$ µm. Here, we assumed $\tan\theta$ to be constant and equal to $\tan\theta_0$, which is a feasible approximation in the vicinity of λ_0, as is shown in Fig. 10.

Since $\tan\theta$ increases with decreasing wavelength, the positive feedback further enhances the resonance wavelength lowering.

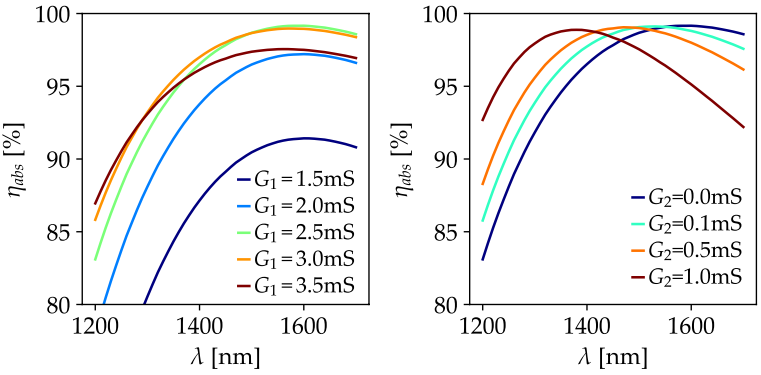

Fig. 7 Optical absorption in nanowire with fixed $G_2 = 0$ *mS* (left) and varying G_1, and with fixed real effective conductance $G_1 = 2.5$ *mS* (right)

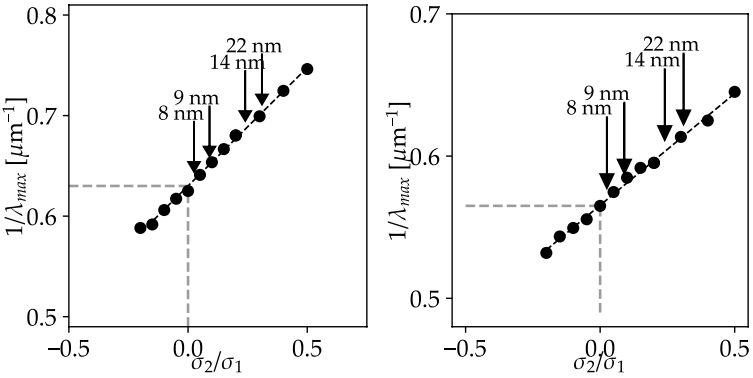

Fig. 8 Dependence of wavelengths of the simulated absorption maxima on the conductivity ratio $\tan\theta = \sigma_2/\sigma_1 = G_2/G_1$, given by samples with different thicknesses. Left: on top of the 250 nm SiO_2 substrate, Right: on top of the 200 nm Si_3N_4 membrane

This simple relation can be directly implemented in the detector design. The absorption maximum shift due to the imaginary part of the conductivity (contribution of the thin film), for a given dielectric layer, limits the possible range of film thicknesses.

However, using e.g. a commercially available 200 nm thick Si_3N_4 membrane, the resonance wavelength determined by the membrane is $4\Lambda \approx 1800$ nm and the corresponding absorption at λ_0 is thus lower, as can be seen in Fig. 8. Using thicker NbN films, the resonance wavelength can be lowered and the absorption can be significantly increased, see Table 3. For each film thickness, the fill factor was optimized to obtain the maximum absorption at λ_0. Thus, fine-tuning the absorption peak position up to 200 nm is possible, without significant loss of total optical absorption η_{abs}.

The fit parameter for the 200 nm Si_3N_4 membrane is $\lambda_c = 6.3\ \mu$m, estimated from the linear fit in Fig. 8.

3.1 Discussion

In similar studies, the properties of a single deposited film are often measured (for example by spectroscopic ellipsometry), and the determined specific conductivity is considered to be thickness-independent in the simulations. Consequently, the nanowire's thickness and width are then tuned to maximize the optical absorption in

Table 3 Sample parameters with simulated maximum absorption at 1550 nm, optimized fill factor for 1550 nm, the wavelength of maximum absorption, and maximum absorption value, respectively

200 nm Si_3N_4, $4\Lambda = 1800$ nm					
d (nm)	σ_2/σ_1 @1550 nm	Max (η_{abs}) @1550 nm (%)	Fill factor	λ_{max} (nm)	Max (η_{abs}) (%)
8	0.025	93.3	0.65	1800	98.8
9	0.092	95.3	0.5	1750	98.7
14	0.242	**98.6**	0.3	1600	98.6
22	0.314	97.5	0.225	1450	98.1

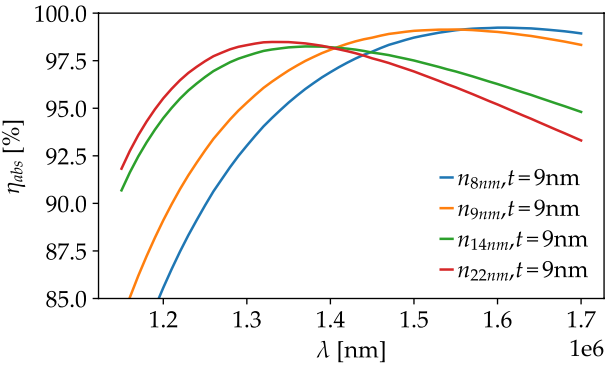

Fig. 9 Simulated optical absorption of 9 nm thick sample on top of the resonant cavity. Other curves show the change in optical absorption of the optical conductivity (refraction index) taken from a sample with different thicknesses

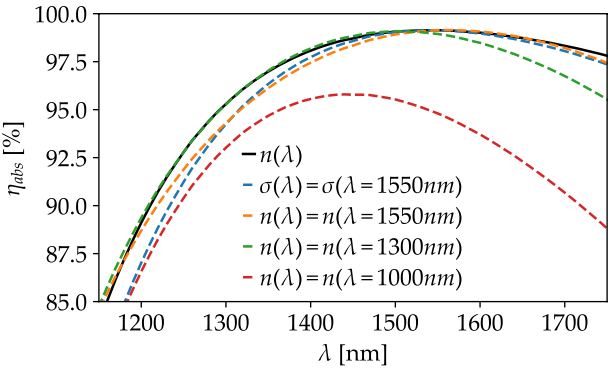

Fig. 10 Simulated absorption of a sample with wavelength dependent $n(\lambda)$, constant $n(\lambda = 1000, 1300, 1550\,\text{nm})$ and n corresponding to constant $\sigma(\lambda = 1550\,\text{nm})$, respectively

the nanowire at the aimed wavelength λ_0. For example, in Ref. Anant et al. (2008), or Ref. Yamashita et al. (2013) the same refraction index was used for samples with thicknesses ranging from 4 to 10 nm, in case of Ref. Zhang et al. (2017) even from 1 to 16 nm. Rescaling the thickness of a specific film to a requested value results in the inaccuracy of the simulated absorption. This fact is acknowledged in Ref. Driessen, E. F. C. et al. (2009), however, no further analysis is present. Rarely, the refractive index is also considered to be wavelength independent (Anant et al. 2008).

To illustrate the error arising from this approximation, we simulated the optical absorption in the above-described nanowire for the respective conductivity $\tilde{\sigma}(t)$, and the corresponding optical indices, given by Eq. 5. For example, using the conductivity of the film with t_{meas} =14 nm and simply rescaling it to $t = 9$ nm for the simulation would result in a decrease of the simulated absorption maxima by approximately 200 nm, as can be seen in Fig. 9.

If one assumes the optical conductivity (refraction index) of these films to be wavelength-independent, the error in the absorption spectra will accumulate with the distance from the reference wavelength, as is shown in Fig. 10.

4 Conclusion

We modeled the absorption spectra of NbN nanowires in a $\lambda/4$ resonator for different film thicknesses and showed that the optical conductivity of thin films significantly affects the absorption spectra. The optical conductivity of disordered metallic films is strongly affected by the presence of quantum corrections, resulting in nontrivial wavelength and thickness dependence of the optical conductivity. The real part of the conductivity determines the amplitude of absorption of the nanowire in the $\lambda/4$ optical resonator, whereas the imaginary part contributes to the wavelength shift of the maxima. The wavelength shift of the absorption maxima can be expressed in terms of the ratio of imaginary and real parts of the optical conductivity, which is a characteristic of a film with a particular thickness. This knowledge can be utilized in detector design and optimization of its optical properties. Thus, to properly simulate and optimize the absorption of the detectors at a required wavelength, it is necessary to work with the precise optical conductivity of the particular layers. These can be obtained by direct measurements of the samples in the required range, or by utilizing a model that describes the optical conductivity of the disordered samples well, as presented in Kern et al. (2024).

Acknowledgements We are grateful for financial support provided by the Slovak Research and Development Agency under the contract APVV-20-0425, and by the project skQCI (101091548), founded by the European Union (DIGITAL) and the Recovery and Resilience Plan of the Slovak Republic.

Author Contributions PN and MB conceptualized the study. Simulations, data curation, and visualization were performed by MB, and optical conductivity analysis by SK, under PN supervision. The draft of the manuscript was written by MB, SK, and PN. Project administration and funding acquisition were provided by MG. All authors read and approved the final manuscript.

Funding Open access funding provided by The Ministry of Education, Science, Research and Sport of the Slovak Republic in cooperation with Centre for Scientific and Technical Information of the Slovak Republic. This work was supported by the Slovak Research and Development Agency under the contract APVV-20-0425, and by the project skQCI (101091548), founded by the European Union (DIGITAL) and the Recovery and Resilience Plan of the Slovak Republic.

Data availability The datasets generated and analysed during the current study are available from the corresponding author upon reasonable request.

Declarations

Conflict of interest The authors have no relevant financial or non-financial interests to disclose.

References

Aktas, D., Fedrici, B., Kaiser, F., Lunghi, T., Labontã, L., Tanzilli, S.: Entanglement distribution over 150 km in wavelength division multiplexed channels for quantum cryptography. Laser Photon. Rev. **10**(3), 451–457 (2016). https://doi.org/10.1002/lpor.201500258

Anant, V., Kerman, A.J., Dauler, E.A., Yang, J.K.W., Rosfjord, K.M., Berggren, K.K.: Optical properties of superconducting nanowire single-photon detectors. Opt. Express **16**(14), 10750–10761 (2008). https://doi.org/10.1364/OE.16.010750

Banerjee, A., Heath, R.M., Morozov, D., Hemakumara, D., Nasti, U., Thayne, I., Hadfield, R.H.: Optical properties of refractory metal based thin films. Opt. Mater. Express **8**(8), 2072–2088 (2018). https://doi.org/10.1364/OME.8.002072

Cabrera, B., Clarke, R.M., Colling, P., Miller, A.J., Nam, S., Romani, R.W.: Detection of single infrared, optical, and ultraviolet photons using superconducting transition edge sensors. Appl. Phys. Lett. **73**(6), 735–737 (1998)

Chang, J., Los, J.W.N., Tenorio-Pearl, J.O., Noordzij, N., Gourgues, R., Guardiani, A., Zichi, J.R., Pereira, S.F., Urbach, H.P., Zwiller, V., Dorenbos, S.N., Esmaeil-Zadeh, I.: Detecting telecom single photons with 99.5–2.07+0.5% system detection efficiency and high time resolution. APL Photon **6**(3), 036114 (2021). https://doi.org/10.1063/5.0039772

Chen, Y.-A., Zhang, Q., Chen, T.-Y., Cai, W.-Q., Liao, S.-K., Zhang, J., Chen, K., Yin, J., Ren, J.-G., Chen, Z., Han, S.-L., Yu, Q., Liang, K., Zhou, F., Yuan, X., Zhao, M.-S., Wang, T.-Y., Jiang, X., Zhang, L., Liu, W.-Y., Li, Y., Shen, Q., Cao, Y., Lu, C.-Y., Shu, R., Wang, J.-Y., Li, L., Liu, N.-L., Xu, F., Wang, X.-B., Peng, C.-Z., Pan, J.-W.: An integrated space-to-ground quantum communication network over 4,600 kilometres. Nature **589**(7841), 214–219 (2021). https://doi.org/10.1038/s41586-020-03093-8

COMSOL (2023) Multiphysics® v. 6.2. https://www.comsol.com. COMSOL AB, Stockholm, Sweden

Driessen, E.F.C., Braakman, F.R., Reiger, E.M., Dorenbos, S.N., Zwiller, V., de Dood, M.J.A.: Impedance model for the polarization-dependent optical absorption of superconducting single-photon detectors. Eur. Phys. J. Appl. Phys. **47**(1), 10701 (2009). https://doi.org/10.1051/epjap/2009087

Efros, A.L., Pollak, M.: Electron-Electron Interactions in Disordered Systems. Elsevier, Amsterdam (2012)

Esmaeil Zadeh, I., Chang, J., Los, J.W.N., Gyger, S., Elshaari, A.W., Steinhauer, S., Dorenbos, S.N., Zwiller, V.: Superconducting nanowire single-photon detectors: a perspective on evolution, state-of-the-art, future developments, and applications. Appl. Phys. Lett. **118**(19), 190502 (2021). https://doi.org/10.1063/5.0045990

Goĺtsman, G.N., Okunev, O., Chulkova, G., Lipatov, A., Semenov, A., Smirnov, K., Voronov, B., Dzardanov, A., Williams, C., Sobolewski, R.: Picosecond superconducting single-photon optical detector. Appl. Phys. Lett. **79**(6), 705–707 (2001)

Hao, H., Zhao, Q., Huang, Y.E.A.: A compact multi-pixel superconducting nanowire single-photon detector array supporting gigabit space-to-ground communications. Light Sci. Appl. **13**(1), 25 (2024). https://doi.org/10.1038/s41377-023-01374-1

Kern, S., Neilinger, P., Poláčková, M., Baránek, M., Plecenik, T., Roch, T., Grajcar, M.: Optical and transport properties of NbN thin films revisited. arXiv preprint (2024). https://doi.org/10.48550/arXiv.2405.03704

Lau, J.A., Verma, V.B., Schwarzer, D., Wodtke, A.M.: Superconducting single-photon detectors in the mid-infrared for physical chemistry and spectroscopy. Chem. Soc. Rev. **52**, 921–941 (2023). https://doi.org/10.1039/D1CS00434D

Lim, H.C., Yoshizawa, A., Tsuchida, H., Kikuchi, K.: Wavelength-multiplexed entanglement distribution. Opt. Fiber Technol. **16**(4), 225–235 (2010). https://doi.org/10.1016/j.yofte.2010.05.001

Marsili, F., Verma, V.B., Stern, J.A., Harrington, S., Lita, A.E., Gerrits, T., Vayshenker, I., Baek, B., Shaw, M.D., Mirin, R.P., Nam, S.W.: Detecting single infrared photons with 93% system efficiency. Nat. Photon. **7**(3), 210–214 (2013)

Neilinger, P., Greguš, J., Manca, D., Grančič, B., Kopčík, M., Szabó, P., Samuely, P., Hlubina, R., Grajcar, M.: Observation of quantum corrections to conductivity up to optical frequencies. Phys. Rev. B **100**, 241106 (2019). https://doi.org/10.1103/PhysRevB.100.241106

Redaelli, L., Bulgarini, G., Dobrovolskiy, S., Dorenbos, S.N., Zwiller, V., Monroy, E., Gérard, J.M.: Design of broadband high-efficiency superconducting-nanowire single photon detectors. Superconduct. Sci. Technol. **29**(6), 065016 (2016). https://doi.org/10.1088/0953-2048/29/6/065016

Renker, D.: Geiger-mode avalanche photodiodes, history, properties and problems. Nucl Instrum Methods Phys Res Sect A Accel Spectrom Detect Assoc Equip **567**(1), 48–56 (2006). https://doi.org/10.1016/j.nima.2006.05.060. Proceedings of the 4th International Conference on New Developments in Photodetection

Ribezzo, D., Zahidy, M., Vagniluca, I., Biagi, N., Francesconi, S., Occhipinti, T., Oxenløwe, L..K., Lončarić, M., Cvitić, I., Sipčević, M., Pušavec, v, Kaltenbaek, R., Ramšak, A., Cesa, F., Giorgetti, G., Scazza, F., Bassi, A., De Natale, P., Cataliotti, F..S., Inguscio, M., Bacco, D., Zavatta, A.: Deploying an inter-European quantum network. Adv. Quantum Technol. **6**(2), 2200061 (2023)

Shibata, H., Honjo, T., Shimizu, K.: Quantum key distribution over a 72 dB channel loss using ultralow dark count superconducting single-photon detectors. Opt. Lett. **39**(17), 5078–5081 (2014). https://doi.org/10.1364/OL.39.005078

Volkov, S., Gregor, M., Roch, T., Satrapinskyy, L., Grančič, B., Fiantok, T., Plecenik, A.: Superconducting properties of very high quality NbN thin films grown by pulsed laser deposition. J. Electr. Eng. **70**(7), 89–94 (2019). https://doi.org/10.2478/jee-2019-0047

Wang, H., Li, H., You, L., Wang, Y., Zhang, L., Yang, X., Zhang, W., Wang, Z., Xie, X.: Fast and high efficiency superconducting nanowire single-photon detector at 630 nm wavelength. Appl. Opt. **58**(8), 1868–1872 (2019). https://doi.org/10.1364/AO.58.001868

Yamashita, T., Miki, S., Terai, H., Wang, Z.: Low-filling-factor superconducting single photon detector with high system detection efficiency. Opt. Express **21**(22), 27177–27184 (2013)

You, L.: Superconducting nanowire single-photon detectors for quantum information. Nanophotonics **9**(9), 2673–2692 (2020). https://doi.org/10.1515/nanoph-2020-0186

Zhang, W., You, L., Li, H., Huang, J., Lv, C., Zhang, L., Liu, X., Wu, J., Wang, Z., Xie, X.: NbN superconducting nanowire single photon detector with efficiency over 90% at 1550 nm wavelength operational at compact cryocooler temperature. Sci. China Phys. Mech. Astron. **60**(12), 120314 (2017). https://doi.org/10.1007/s11433-017-9113-4